Faraday Discussions

Volume 195

Reaction Rate Theory

ROYAL SOCIETY
OF CHEMISTRY

PAPER

Reactive trajectories of the Ru$^{2+/3+}$ self-exchange reaction and the connection to Marcus' theory

Ambuj Tiwari[ab] and Bernd Ensing*[abc]

Outer sphere electron transfer between two ions in aqueous solution is a rare event on the time scale of first principles molecular dynamics simulations. We have used transition path sampling to generate an ensemble of reactive trajectories of the self-exchange reaction between a pair of Ru^{2+} and Ru^{3+} ions in water. To distinguish between the reactant and product states, we use as an order parameter the position of the maximally localised Wannier center associated with the transferring electron. This allows us to align the trajectories with respect to the moment of barrier crossing and compute statistical averages over the path ensemble. We compare our order parameter with two typical reaction coordinates used in applications of Marcus theory of electron transfer: the vertical gap energy and the solvent electrostatic potential at the ions.

Introduction

Electron transfer is the fundamental process in reduction and oxidation (*i.e.* redox) chemistry, taking place for example in metal corrosion, fuel cell reactions, and photo-synthesis. Early pioneering studies of the prototypical self-exchange reaction between two metal ions in aqueous solution, as illustrated by eqn (1),

$$M^{n+} + M*^{(n+1)+} \rightarrow M^{(n+1)+} + M*^{n+} \tag{1}$$
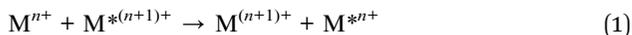
have been pivotal for our understanding of electron transfer processes and the development of Marcus' theory of electron transfer.[1–4] Molecular dynamics (MD) and Monte Carlo simulations confirmed that the free energy profiles of electron transfer reactions consist of two intersecting parabolas, as proposed by Marcus' theory, confirming that the solvent reorganisation during electron transfer is indeed well-described by the linear response approximation.[5–11]

aVan't Hoff Institute for Molecular Sciences, Universiteit van Amsterdam, Science Park 904, 1098 XH Amsterdam, The Netherlands. E-mail: b.ensing@uva.nl

bAmsterdam Center for Multiscale Modeling, Science Park 904, 1098 XH Amsterdam, The Netherlands

cCatalan Institute of Nanoscience and Nanotechnology (ICN2), CSIC and The Barcelona Institute of Science and Technology, Campus UAB, Bellaterra, 08193 Barcelona, Spain

As with most chemical reactions, the self-exchange reaction is an activated process, in which the system has to surpass a transition state of high (free) energy, which renders direct sampling of an electron transfer reaction in an MD simulation highly improbable. This so-called *rare event* problem was tackled in the early work by using enhanced sampling techniques, such as umbrella sampling[6,7] or free energy perturbation,[10] which bias the simulation along an appropriate reaction coordinate, for example the position of the electron.

Unfortunately, it is not so easy to bias the electron transfer process in combination with a quantum-chemical many-electron description of the system, such as with density functional theory (DFT). The reason is that the position of the excess electron, in the reactant state, the product state, or somewhere in between, is governed by the configurational state of the polar solvent environment, which is difficult to capture with a reaction coordinate. The method of constrained-DFT[12–14] offers alternatively the possibility to use the electron position as the reaction coordinate, although this constraint also confines the orbital to a certain shape.

Instead, most DFT studies on electron transfer focus on half-reactions. With the half-reaction approach, introduced by Warshel,[5,10] and further developed for DFT-MD simulation by Sprik and co-workers,[15–20] the redox potential and reorganisation free energy is computed from the average energy needed to add (or remove) an electron to (or from) the system containing only the solvated donor or acceptor species. This approach has been extensively applied to investigate the redox properties of transition metals,[16–19,21,22] organic molecules,[20,23–25] and proteins[26,27] in explicit solvent. However, the half-reaction approach does not provide direct information on the electron transfer between a donor and acceptor species, such as their average distance, as the model only considers one of the two species at once.

We have recently returned to the problem of direct simulation of electron transfer between donor and acceptor species with DFT-MD.[28] Using transition path sampling (TPS) simulations,[29,30] we can generate an ensemble of reactive trajectories that sample the unbiased dynamics of an electron transfer process. Analysis of the trajectories provides unique information on the transition state ensemble, such as the donor–acceptor distance, the solvent structure in the transition state and the dynamics of the process. Particularly interesting would be an analysis of relevant order parameters or collective variables that correlate with the vertical energy gap, ΔE, which is the reaction coordinate used in Marcus theory. However, direct computation of ΔE is difficult within the DFT-MD simulations, as it requires constraining the position of the electron.

Here, we analyse a DFT-MD/TPS ensemble of reactive trajectories of the self-exchange reaction between a pair of Ru^{2+} and Ru^{3+} ions in water solvent. Rather than computing ΔE, we obtain statistics of the energy to insert or delete an electron (ΔE^{ins}, ΔE^{del}) to the system along the reactive trajectory. We first sample these two vertical gap energies for the pair of Ru^{2+} and Ru^{3+} ions in an equilibrium simulation to reconstruct the free energy landscape, which we compare to that obtained using the half-reaction approach. We then sample ΔE^{ins} and ΔE^{del} along the reactive trajectories, and compare the sum as a reaction coordinate to the solvent electrostatic potential and an order parameter based on the position of the transferring electron.

In the following, we first briefly summarise the theory of electron transfer as applied in half-reaction simulations, we discuss the issues associated with the use of periodic boundary conditions, and we present the computational details of our combined transition path sampling and DFT-MD simulations. The results are presented in three subsections covering the redox properties obtained with the half-reaction approach, our equilibrium DFT-MD simulations of the pair of Ru^{2+} and Ru^{3+} ions in water, and analysis of the reactive trajectories of the electron transfer obtained with TPS. This is followed by the conclusions.

1 Methods

1.1 Theory of electron transfer

At the DFT level of theory, redox properties of ions and molecules in explicit solvent are most conveniently computed using the half-reaction approach, which is based on Marcus' theory of electron transfer and can be connected to the half-reactions that take place in electrochemical cell experiments. The central quantity to be measured is the vertical energy gap, ΔE, which is the energy needed to add (or delete) an electron to (or from) the solute in a given nuclear configuration. This gap energy plays the role of the reaction coordinate and it quantifies the state of the polarised medium when the solute is an ion. In the case of a molecular solute, ΔE also captures the state of the molecule itself. In remarkably many cases (but not always[25]), the response of both the polarised medium and the molecular solute, as measured by ΔE, is largely linear with respect to the amount of charge loaded to or from the solute.

Consider the reduction of an oxidant (O) to a reductant (R),

$$O + e^- \rightarrow R, \tag{2}$$

and the vertical energy gap

$$\Delta E = E_R(\mathbf{r}^N) - E_O(\mathbf{r}^N), \tag{3}$$

with $E_x(\mathbf{r}^N)$, $x = (R, O)$, the internal energy of the system at a nuclear configuration $\mathbf{r}^N$, in the reduced or oxidised state, respectively. Linear response of the system entails that the distribution $P(\Delta E)$ is Gaussian, centered at an (ensemble) average $\langle \Delta E \rangle_x$ in either the reduced or oxidised state:

$$P_x(\Delta E) = \frac{1}{\sigma_x \sqrt{2\pi}} \exp\left[- \frac{(\Delta E - \langle \Delta E \rangle_x)^2}{2\sigma_x^2} \right], \tag{4}$$

with σ^2 the variance. The Landau free energies, as a function of the ΔE reaction coordinate,

$$\Delta A_x(\Delta E) = -k_B T \ln[P(\Delta E)], \tag{5}$$

must then be parabolic and give rise to Marcus' well-known diabatic free energy landscape, which is illustrated in Fig. 1 by the dashed curves. Here, T is the temperature and k_B is Boltzmann's constant.

The overall reaction free energy is a particularly simple function of the average gap energies when linear response holds:
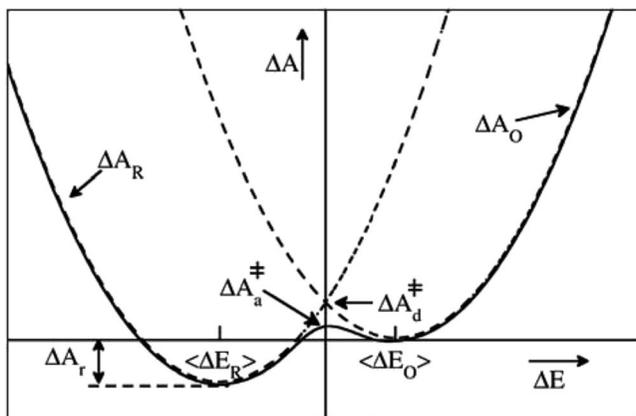
Fig. 1 Schematic illustration of a parabolic free energy landscape of electron transfer. The dashed lines depict Marcus' diabatic free energy curves, which cross at the diabatic free energy barrier $\Delta A_d^\ddagger$. The solid line shows the adiabatic free energy profile, with a somewhat lower barrier $\Delta A_a^\ddagger$, due to the coupling of the electronic reactant and product states. The difference between $\Delta A_d^\ddagger$ and $\Delta A_a^\ddagger$ is generally much smaller than depicted here. For a half-reaction written in the conventional reduction form (eqn (2)) and the definition of the reaction coordinate, ΔE, from eqn (3), the reaction thus takes place from right to left.

$$\Delta A_r = \frac{1}{2}\left(\langle\Delta E\rangle_O + \langle\Delta E\rangle_R\right), \tag{6}$$

and a similar relation holds for the third key quantity in Marcus' theory, the reorganisation free energy:

$$\lambda = \frac{1}{2}\left(\langle\Delta E\rangle_O - \langle\Delta E\rangle_R\right), \tag{7}$$

This λ is the free energy associated with the relaxation of the polarised medium into the product state after a vertical excitation, *i.e.* after adding an electron to the solute at a fixed configuration. The reorganisation free energy is also associated to the curvature of the free energy curves and to the magnitude of the fluctuations of ΔE in either oxidation state:

$$\lambda_x = \frac{\sigma_x^2}{2k_B T} \tag{8}$$

Finally, the diabatic free energy barrier, denoted in Fig. 1 at the crossing point of the parabolas, is given as a function of the overall reaction free energy (which is zero for a full self-exchange reaction, but not for the half-reaction) and the reorganisation free energy:

$$\Delta A_d^\ddagger = \frac{(\lambda + \Delta A_r)^2}{4\lambda}. \tag{9}$$

In practice, the diabatic free energy curves are computed by sampling ΔE along two equilibrium DFT-MD simulations; one in the oxidised state where the energy needed to add an electron is computed and one in the reduced state in which the energy to delete an electron is sampled. In Section 2.1, we will set the stage by

applying this approach to compute the redox properties of the Ru^{2+}/Ru^{3+} couple, which can be compared to the extensive studies on this system by Blumberger and Sprik.[17–19,22,31]

As pointed out in the introduction, the half-reaction framework cannot be so easily applied to study directly the full reaction, *i.e.* the electron transfer reaction between a donor molecule and an acceptor molecule. In the full reaction case, ΔE would be the energy to bring the electron from the donor to the acceptor at a fixed configuration. This ΔE can be decomposed into two terms: (1) the energy needed to delete the electron from the donor, ΔE^{del}, and (2) the energy needed to insert the electron at the acceptor, ΔE^{ins}. The first term is easy to compute as long as the transferring electron resides at the highest occupied orbital (HOMO) of the system. But the second term cannot be computed with ground-state DFT without additional constraints, since the electron would return to the donor in the electronic ground-state. Of course, we can compute the energy needed to insert an electron at the acceptor before removing the electron from the donor, $\Delta E^{ins,before}$, but that energy would contain an additional interaction energy of the inserted electron with the other electron still at the donor, plus higher order terms in a polarisable environment.

If we consider this additional electron interaction as a correction to the $\Delta E^{ins,before}$ term, the ΔE of moving an electron from donor to acceptor at a given nuclear configuration can thus be computed using the half-reaction technique of inserting an electron and deleting an electron:

$$\Delta E = \Delta E^{del} + \Delta E^{ins} + U^{corr}. \tag{10}$$

Here, and hereafter, we omit the "before" superscript; that is, the ΔE^{ins} refers to the energy needed to insert an electron into the original system instead of the system after having deleted an electron from the donor. As an initial approximation, the correction term could be taken as the Coulomb energy between an electron centered at the donor and an electron centered at the acceptor:

$$U^{corr} = \frac{1}{4\pi\varepsilon_0} \frac{1}{|\mathbf{r}_{Ru_D} - \mathbf{r}_{Ru_A}|} \tag{11}$$

However, due to the periodic boundary conditions applied in these calculations, the correction is somewhat more complicated, as further discussed next.

1.2 Periodic boundary conditions and finite size effects

One of the complications of DFT-MD simulations of molecular processes in condensed materials, and in particular of half-reactions in aqueous solution, is related to the rather small size of the systems and the periodic boundary conditions to mimic the extended phase. The long-range electrostatic interactions are computed using Ewald summation, which is of course almost always much better than using a cutoff, but is nevertheless not without its own issues. The problem is that the half-reaction approach is typically applied to systems that are not neutral, and, moreover, the method requires the calculation of energy differences between systems that carry different charges.

Although in principle a charged system embedded in infinite arrays of periodic copies would have an infinite energy, Ewald summation removes the divergent term in a manner that is commonly interpreted as adding a uniformly smeared

out background charge. The density of the background charge is $-q/L^3$ and thus depends on the box size, L. The charged system interacts with the background charge so that the energy of the system contains a "self-interaction" term that is a function of the box size and shape. For a charged particle in a cubic cell, this (Wigner) self-interaction is:

$$\Phi = - \frac{\xi_M q^2}{2L} \tag{12}$$

with q the charge of the particle, L is the cell dimension, and $\xi_M = 2.837297$ the Madelung constant of a cubic periodic system. The finite size effects due to the Ewald potential have been extensively investigated, for example for the interaction energy between two ions,[32] for ionic hydration free energies,[33–35] for the reaction and reorganisation free energies in half-reaction calculations by Sprik,[19,24] and by Blumberger[22] on the reorganisation free energy in (full reaction) electron transfer.

For a charged particle dissolved in a polar medium such as water, it turns out that the self-interaction energy is largely compensated by the screening of the solvent, effectively reducing this L^{-1} dependent term by a factor of $1/\varepsilon$, with ε the dielectric constant, which is approximately 80 for ambient water. The L^{-1}-dependence of the solvent comes from the repulsion of the polarised solvent in the unit cell with that in the periodic images, which solvate the periodic image of the charged particle in their own cell, rather than the original ion.

Although the L^{-1}-dependent self-interaction is thus largely canceled in a high-dielectric solvent, higher order terms in L remain that arise from the finite size of the ion, which creates a cavity with a radius R in the medium in all periodic images. The total energy difference due to (Ewald) periodic boundary conditions (PBC) with respect to that of a continuum Bohr model[19,34,35] (B) is:

$$E_{PBC} - E_B = \frac{\xi_M q^2}{2L\varepsilon} - \left(1 - \frac{1}{\varepsilon}\right)\frac{2\pi q^2 R^2}{3L^3} + O(L^{-5}) \tag{13}$$

In the half-reaction approach presented above, the reaction free energy, ΔA_r (eqn (6)), and the reorganisation free energy, λ (eqn (7)), are computed from sampled energy differences, ΔE, of the system with and without an extra charge. Sprik *et al.* found that for ΔA_r the box size dependence is dominated by the L^{-3} term, whereas λ scales as L^{-1}. Blumberger and Lamoureux showed that for the full electron transfer reaction, in which the electron moves from donor to acceptor, the box size dependence of the reorganisation free energy is much less severe. This is perhaps not surprising, since in that case only the dipole is changed, but not the total charge.[22]

The dipole term depends on the distance between the donor and the acceptor. In Fig. 2, we show the $P(\Delta E^{ET})$ (top panel) and the free energy curve computed with eqn (5) (bottom panel) computed with simple force field MD simulations of a pair of Ru^{2+} and Ru^{3+} aqua complexes, constrained at different donor–acceptor distances, d, ranging from 6 to 14.5 Å, solvated in 1000 water molecules in a cubic box with $L = 31.04$ Å. As expected, the curves show a clear dependence on the donor–acceptor distance.

The black curves in Fig. 2 were computed using the insertion–deletion scheme, with $\Delta E^{del+ins} = \Delta E^{del} + \Delta E^{ins}$, *i.e.* the first two terms of eqn (10), which are, within
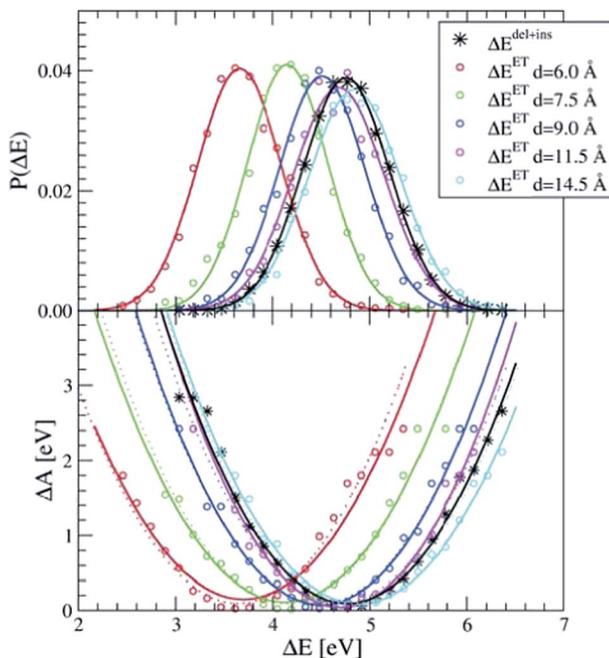
Fig. 2 The apparent dependence on the distance between the Ru^{2+} and Ru^{3+} ions of the energy gap probability (top) and the free energy curves (bottom) computed with force field MD simulations. The curves obtained from $\Delta E^{del+ins}$ (in black) are not distance dependent. The lines are Gaussian (top) and parabolic (bottom) fits through the measured data (circles). Dashed lines in the bottom panel are computed by adding to $\Delta E^{del+ins}$ the U^{corr} term of eqn (10) as explained in the text.

the statistical accuracy, independent of the Ru–Ru distance. The missing U^{corr} term of eqn (10) can be computed as the difference in $\Delta E^{del+ins}$ between a system containing the two ruthenium point charges (without solvent) with, and without, periodic boundary conditions. Adding this to the $\Delta E^{del+ins}$ indeed recovers perfectly the ΔE^{ET} curves, as shown by the dotted lines in the bottom panel of Fig. 2.

For the DFT-MD simulations that we discuss hereafter, the box size dependence and the U^{corr} term also contain contributions due to the instantaneous electronic polarisation. The aim of this work, however, is not to obtain quantitative numbers for the redox properties, but rather, to connect the reaction coordinates used in Marcus theory and the half-reaction method to our equilibrium and TPS simulations of the full electron transfer reaction.

1.3 Transition path sampling

We use an adapted 2-way TPS algorithm of shooting and shifting moves to generate reactive trajectories, starting from an initial path obtained from a biased MD simulations as explained hereafter. Here, reactive trajectory refers to a trajectory that starts in the stable reactant state and ends in the stable product state, or *vice versa*. The shooting move proceeds in the usual way. That is, each new trajectory starts from a randomly chosen configuration from the previous

trajectory, by adding small perturbations to all atomic momenta, and performing two MD simulations, one forward and one backward (by reversing all velocities) in time (hence, "2-way TPS"). The shooting move is accepted if the new trajectory connects the reactant and product states, or rejected otherwise. The perturbations are done by adding random momenta from a 5 Kelvin Maxwell–Boltzmann distribution to the original momenta, removing any total momentum, and rescaling to the original temperature. This resulted in an average acceptance ratio of the shooting move of 0.46. Instead of the original shifting move, we locate the configuration on the previous trajectory that is closest to halfway for the electron transfer process. The shooting configuration was subsequently chosen from a fixed number of saved restart files ranging from 1000 MD steps (*i.e.* 500 fs) before and after this central time frame. By using this fixed number of restart files to randomly choose the shooting configuration from, the TPS algorithm obeys detailed balance. The actual trajectory length was not fixed however, and ranged typically between 2 and 3 ps.

The initial reactive trajectory was obtained from a 1 ps constrained MD simulation that started from an equilibrated system, in which the six ruthenium–oxygen distances of the hexaaqua Ru^{2+} complex were forced to decrease by 0.3 Å. By the time that the constrained coordination shell becomes smaller than that of the (free) Ru^{3+} complex, an electron is expelled from the Ru^{2+} complex and taken up by the Ru^{3+} complex soon after. A second constrained simulation was initiated from a frame just after the forced electron transfer took place, in which the six Ru–O distances were kept constant. This second trajectory was used to generate initial unconstrained reactive trajectories, by applying the TPS shooting move but without perturbing the nuclear momenta.

The stable reactant and product states are defined by the numbers of d-electrons at each of the ruthenium ions; six on one and five on the other, or *vice versa*. Counting the number of electrons is conveniently done by transforming the occupied orbitals into maximally localised Wannier functions[36,37] (MLWFs) and computing the distances of the MLWF centers to each of the Ru ions. The MLWFs are computed every 10 MD steps on-the-fly along each TPS trajectory. We define as an order parameter:

$$\xi_{ET} = (d_{Ru–X} - d_{Ru'–X})/d_{Ru–Ru'}, \tag{14}$$

in which Ru and Ru′ denote the two Ru ions, d is the distance and X is the MLWF that is, of the eleven MLWF centers within a cutoff distance of the Ru nuclei, farthest away. This order parameter is practically equal to minus one in the reactant state with the first Ru ion being 2+ and the second Ru′ ion is 3+; in the product state with the charges reversed, $\xi_{ET} \approx 1$; and during electron transfer, ξ_{ET} has a value in between. Now, we define the reactant state as the set of configurations for which $\xi_{ET} < -0.9$ and the product state as the set of configurations for which $\xi_{ET} > 0.9$.

The TPS algorithm of generating reactive trajectories described here was implemented using a bash script that would launch the forward and backward DFT-MD simulations (further detailed below), accept or reject the trajectories, choose a new starting configuration, perturb the momenta, and launch the next simulations, and so forth.

1.4 Density functional theory-based molecular dynamics

The DFT-MD simulations were performed using the CP2K software package.[38] The electronic structure part of CP2K, called QUICKSTEP,[39] uses the combined Gaussian and plane-wave (GPW) method[40] for the calculation of forces and energies. The GPW method is based on the Kohn–Sham formulation of density functional theory and employs a hybrid scheme of Gaussian and plane wave functions. First principles simulations with CP2K sample directly the Born–Oppenheimer surface.

In the DFT-MD simulations, the norm-conserving pseudopotentials of Goedecker *et al.* (GTH)[41] were applied to replace the core electrons. We employed the BLYP[42,43] exchange–correlation functional, augmented with Grimme's D2 dispersion correction[44,45] to include van der Waals interactions. The BLYP-D level of theory has been extensively used and tested by the scientific community for the description of various structural and dynamical properties of liquid water and aqueous solutions (see *e.g.* ref. 46 and 47), including the $Ru^{2+/3+}$ redox couple.[17] The Gaussian basis set consisted of a double-zeta valence basis set with a single set of polarisation functions (DZVP) optimised for the use with the GTH pseudopotentials. A charge density cutoff of 280 Ry was used for the auxiliary plane-wave basis set. For the plane-wave grid, we applied the nearest neighbour smoothing operator NN10. A CSVR thermostat[48] with a time constant of 500 fs was used to generate an NVT ensemble. The temperature was set to 300 K. Periodic boundary conditions were applied to a cubic box with an edge length of 12.4138 Å for the simulations with two Ru ions and 64 water molecules. For the single ion with 32 water molecules, the box dimension was 9.86 Å. The simulations here were carried out on the Dutch national supercomputer Cartesius using 24 processors in parallel.

2 Results

We first compute the redox properties of the Ru^{2+}/Ru^{3+} couple using the half-reaction approach. Next, we investigate the pair of aqueous Ru^{2+} and Ru^{3+} ions in equilibrium. Thirdly, we analyse the reactive trajectories of the self-exchange reaction harvested with TPS.

2.1 Redox properties using the half-reaction approach

The Ru^{2+}/Ru^{3+} redox couple was one of the first systems to which Sprik and co-workers applied their half-reaction approach. Here we present the same redox properties computed with the CP2K program at the BLYP+D2/DZVP/280 Ry level of theory for a single ion with 32 water molecules in a cubic box with an edge of L = 9.86 Å subject to periodic boundary conditions. Two equilibrium DFT-MD simulations were performed, one of Ru^{2+} and one of Ru^{3+}, with a length of 10 ps, of which the last 5 ps were used to sample ΔE.

The $P(\Delta E)$ distributions are shown in the top-panel of Fig. 3. The histograms of ΔE, shown by the circles are fitted very well by Gaussian functions (solid lines), as expected, however, the widths of the two distributions, measured by σ, are not exactly the same. The Ru^{2+}/Ru^{3+} system is known to obey Marcus linear response theory rather well,[17–19,22,31] so the deviation seen here must be due to statistical errors.
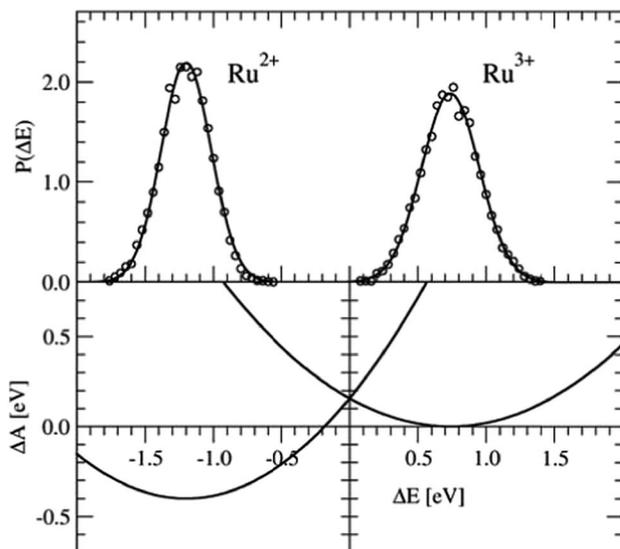
Fig. 3   Top panel: Vertical energy gap distributions for the $Ru^{3+} + e^- \rightarrow Ru^{2+}$ half-reaction. The circles show the histogram values obtained from the simulation data; the solid lines are Gaussian fit functions. Bottom panel: Free energy curves obtained from the Gaussian functions using eqn (5).

The derived redox properties are compiled in Table 1. The uneven standard deviations of ΔE in the oxidised and reduced states leads to a significant discrepancy between λ_O and λ_R. We have previously seen that the fluctuations in ΔE are easily underestimated in the rather short DFT-MD simulations, and that λ computed from the averages (eqn (7)) is the safer estimate for the reorganisation free energy.[25] Our results are in reasonable agreement with the early work of Blumberger and Sprik, although in that work an external chemical potential was applied to enforce alignment of the minima of the parabolic curves, and the parabola were fitted to the combined O and R data-sets resulting in a more symmetric free energy landscape.

Table 1   Average and standard deviations of the computed $P(\Delta E)$ distributions using the half-reaction approach, together with the derived redox properties using the indicated equations

Quantity	Value [eV]	Equation
$\langle \Delta E_R \rangle$	−1.23	(4)
$\langle \Delta E_O \rangle$	0.74	(4)
σ_R	0.18	(4)
σ_O	0.22	(4)
ΔA_r	−0.24	(6)
λ	0.98	(7)
λ_R	0.64	(8)
λ_O	0.93	(8)

2.2 Free energy curves of the combined Ru^{2+} and Ru^{3+} ions

Four independent DFT-MD simulations were performed for a pair of Ru^{2+} and Ru^{3+} ions solvated by 64 water molecules in a cubic box with $L = 12.41$ Å subject to periodic boundaries. These simulations had different starting configurations, but they had in common that in all cases the Ru^{3+} complex was deprotonated. From two of the simulations, we removed at the start the excess proton from the solvent, yielding a total charge of +4 for the system. The other two systems had a charge of +5. In the latter, the extra proton diffused through the solvent *via* the Grotthuss mechanisms, and was not seen to jump back onto the deprotonated ruthenium complex during the simulation. Rather than adding explicit counter ions, which would make the sampling more cumbersome, the system has a neutralising uniform background counter-charge *via* the Ewald summation, as further detailed in the Methods section. The simulations had a length of 50 ps, of which the last 30 ps were used for analysis.

Fig. 4 shows in the top panel the distributions, $P(\Delta E^{del})$ (red curve), $P(\Delta E^{ins})$ (blue), and $P(\Delta E^{del+ins})$ (black). The solid lines are Gaussian functions fitted to the histograms of the data, which are shown in circles for the system without the solvated proton. The fitted Gaussian functions are also shown for the system with the excess proton, with dashed lines, to illustrate that the computed distributions
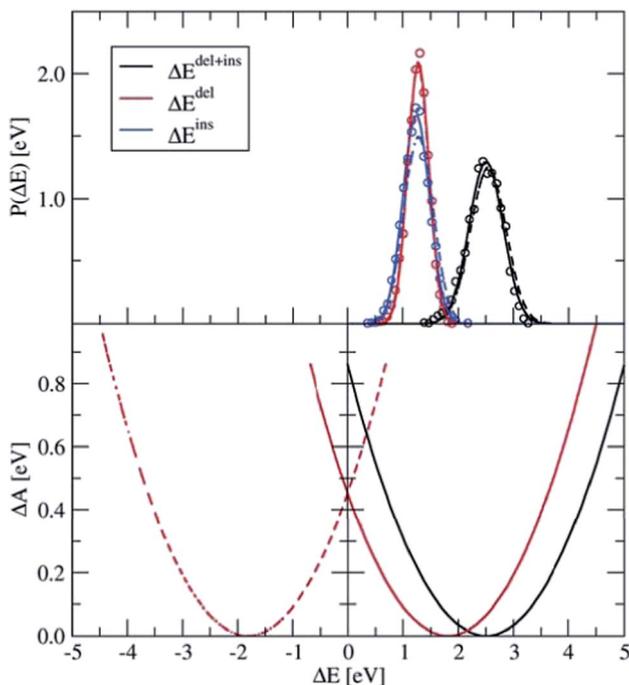

Fig. 4 Top panel: Distributions of ΔE^{del}, ΔE^{ins}, and $\Delta E^{del} + \Delta E^{ins}$, computed for the Ru^{2+} + Ru^{3+} system (circles), which are fitted by Gaussian functions (lines). The solid lines show the results for the 4+ charged system, from which the excess proton was removed; the dashed line shows the results for the 5+ charged system. Bottom panel: Parabolic free energy curve obtained from the Gaussian fit function (solid black line) using eqn (5) and the final free energy curves (red) that are shifted based on $\lambda_{del+ins}$ as explained in the text.

are remarkably independent from the total charge of the system; apart from a small deviation between the blue curves, the distributions obtained from the two systems are, considering the statistical uncertainty, equal to each other.

The distribution of the energy needed to insert an electron at the Ru^{3+} ion is somewhat broader than that of the energy needed to delete an electron at the Ru^{2+} ion. This trend is in agreement with what we found earlier for the $P_O(\Delta E)$ and $P_R(\Delta E)$ distributions with the half-reaction approach (see Fig. 3), although this is probably a coincidence. The more plausible cause for the different widths is the different coordination shells of the Ru^{2+} and Ru^{3+} ions here, the former being coordinated by six water ligands whereas the latter contains five water ligands and one hydroxo ligand. This difference between the oxidised and reduced Ru ions could indeed cause such a non-linear effect.

The first and second moments of the distributions, together with the derived reorganisation free energies are listed in Table 2. The average energy to delete an electron from the system is in perfect agreement with $-\langle \Delta E_R \rangle$ of the half-reaction (Table 1) and also σ matches very well. However, this must be somewhat fortuitous, considering the different box sizes and the effect that the nearby Ru^{3+} complex must have in the current case of the full reaction. Also σ_{ins} is in excellent agreement with σ_O of the half-reaction, however the average $\langle \Delta E^{ins} \rangle$ is significantly shifted with respect to $\langle \Delta E_O \rangle$. This discrepancy is mainly due to the different coordination shells between the Ru^{3+} complexes, which contain a hydroxo ligand in the current full reaction case, while for the half-reaction none of the water ligands were deprotonated.

The lower panel of Fig. 4 shows the parabolic free energy profile obtained from the $P(\Delta E^{del+ins})$ distribution, using eqn (6) (solid black line). Note however, that this profile is shifted with respect to that of the actual electron transfer from Ru^{2+} to Ru^{3+}, as we did not include the correction term, U^{corr}, from eqn (10). But since $\Delta A_r = 0$ for the self-exchange reaction, the average $\langle \Delta E \rangle$ must equal $\lambda_{del+ins}$. Here we neglect the fluctuation part of the correction term, which is expected to be small. In Fig. 4, the shifted free energy curve is shown in red, together with its counterpart of the reverse electron transfer reaction (red dashed). The obtained reorganisation free energy, $\lambda_{del+ins} = 1.73$ eV is in reasonable agreement with

Table 2 Average and standard deviations of the computed $P(\Delta E^{del})$, $P(\Delta E^{ins})$, and $P(\Delta E^{del+ins})$ distributions, together with the derived redox properties using the indicated equations

Quantity	Value [eV]	Equation
$\langle \Delta E^{del} \rangle$	1.23	(4)
$\langle \Delta E^{ins} \rangle$	1.19	(4)
$\langle \Delta E^{del+ins} \rangle$	2.42	(4)
σ_{del}	0.19	(4)
σ_{ins}	0.23	(4)
$\sigma_{del+ins}$	0.30	(4)
ΔA_r	0.0	(6)
λ	2.42	(7)
λ_{del}	0.73	(8)
λ_{ins}	1.05	(8)
$\lambda_{del+ins}$	1.73	(8)

earlier estimates using constrained-DFT (1.62 eV),[31] static quantum-chemistry methods (1.95 eV),[49] and experimental measurement (2.0 eV).[50] Finally, the diabatic free energy barrier for the Ru^{2+}/Ru^{3+} self-exchange reaction is computed with eqn (9) to be $\Delta A_d^{\ddagger} = 0.43$ eV.

2.3 Transition path sampling

We employed the TPS technique in combination with DFT-MD to generate in total eight sequences of reactive trajectories of the self-exchange reaction between a Ru^{2+} ion and a Ru^{3+} ion in water. During the initial constrained MD simulations to generate an initial path (as explained in the Method section), not only an electron transferred, but also a proton was donated by one of the aqua ligands of the Ru^{3+} complex to the solvent. The first four TPS sequences were generated with this proton in the water solvent. The second four TPS sequences were generated after removal of the solvated proton. The first seven sequences contain 50 reactive trajectories. A typical "path tree" of such a sequence is shown in Fig. 5. The eighth sequence contained 180 (accepted) paths. The acceptance ratio over all paths was 0.46. The simulation length of each forward or backward path ranged from 0.5 to 1.5 ps, as seen from the path tree.

Fig. 6 shows a cartoon of snapshots from a representative reactive trajectory. The octahedrally coordinated ruthenium complexes are shown in ball-stick representation (Ru is blue, O is red, and H is white), while the other solvent water
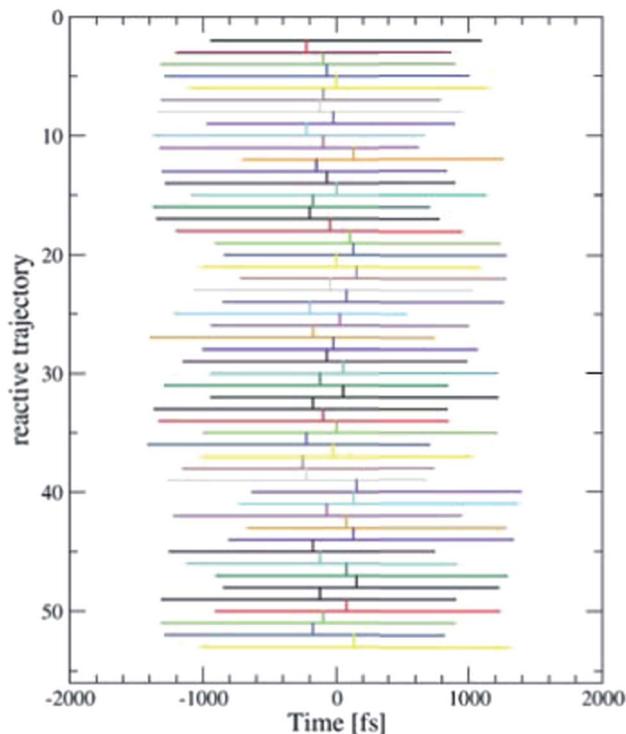

Fig. 5 One of the eight TPS "path trees", showing the length of each path and the shooting time where the next path branches off a previous one. Only the accepted paths are shown.
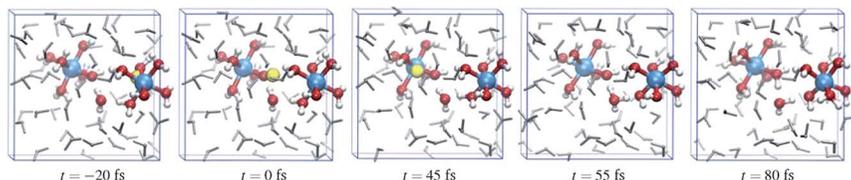
Fig. 6 Five snapshots from a typical reactive trajectory showing the electron transfer represented by the departure of its Wannier center (yellow sphere) from the Ru^{2+} ion (right-hand-side blue sphere) in the left-most panel. In the second panel, the Wannier center is approximately in the middle ($t = 0$), and 45 fs later it arrives at the other Ru ion. A proton from the right-hand-side hexaaqua complex is transferred *via* an intermediate solvent water (fourth panel) to the other complex. Ligands and the intermediate H_2O molecule are shown in red and white ball-and-stick representation; other solvent molecules are drawn as grey sticks.

molecules are shown as grey sticks. In the first panel the Wannier center is seen, as a yellow sphere, to depart from the Ru^{2+} ion. The Ru^{3+} complex on the left side has five water ligands and one hydroxo ligand, which points toward the electron donor complex and is hydrated by a solvent water molecule also drawn in ball-stick representation. In the second panel, the Wannier center is halfway between the donor and acceptor complexes, and 45 fs later the electron is taken up by the acceptor species in panel 3. Panels 4 and 5 show the subsequent proton transfer from the (hitherto) Ru^{2+} complex to the acceptor complex, *via* a bridging solvent water molecule.

The distance between the Ru ions fluctuates around 7 Å. The electron transfer is in all reactive trajectories accompanied by the proton transfer, in no preferential order (as should be expected by time-reversibility). Further details of this proton-coupled electron transfer mechanism are discussed in a separate publication;[28] instead here we will focus on how we can connect the reactive trajectories of the adiabatic electron transfer to the redox quantities from Marcus theory.

In order to perform a statistical analysis over the TPS sequences of reactive trajectories, we have to align the trajectories by time. We take the moment of electron transfer in each path as the zero of the time scale, which we compute by fitting the reaction coordinate values ξ_{ET} (see eqn (14)) along each trajectory by the switch function $f(t) = \tanh[a \times (t - t_0)]$, with the parameter t_0 defining the moment of electron transfer. Fig. 7 shows ξ_{ET}, which quantifies the position of the Wannier center, for three trajectories. Also the average ξ_{ET} over the sequence of 180 paths is shown (black line). The blue line shows a reactive event in which the electron recrossed back toward the donor and again to the acceptor moiety. However, such barrier recrossings are rather scarce in this electron transfer process. Seen from the average ξ_{ET}, the actual electron transfer, that is, passing from the reactant state definition to the product state definition takes about 10^2 fs.

Having aligned the trajectories, statistics of other order parameters can be obtained from the TPS ensemble. Panels B and C of Fig. 7 show ΔE^{del}, ΔE^{ins}, and $\Delta E^{del+ins}$, computed from $t = -0.5$ to $t = 0.5$ ps. The fluctuations seen in the three individual path traces are very large just before and after the electron transfer event, however around $t = 0$ they all show a clear spike toward zero. Only for a few
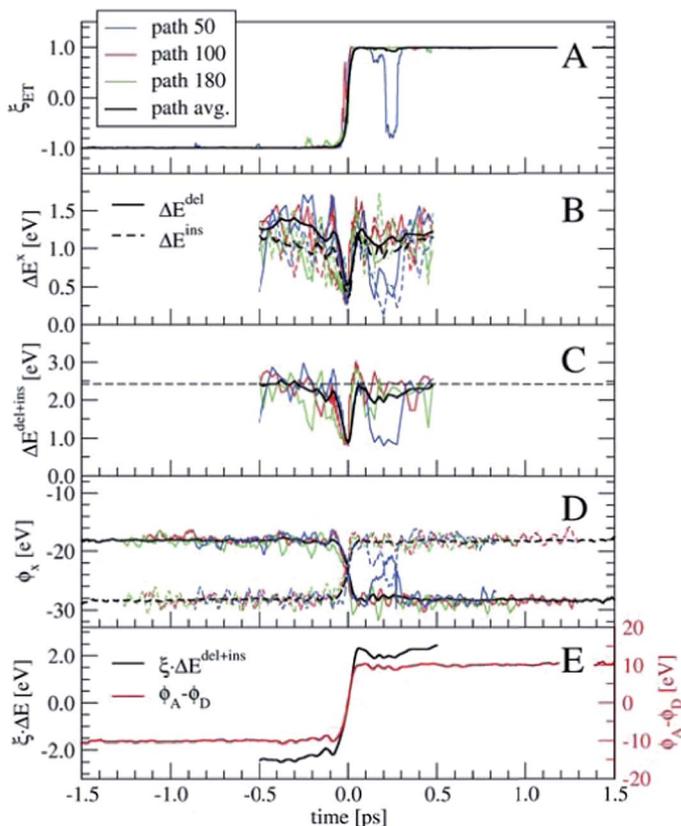
Fig. 7 Panel A: the Wannier center coordinate, ξ_{ET} showing the fast switch from -1 to 1 during electron transfer. Curves for three reactive trajectories are shown, together with the path average. In path 50, a barrier recrossing is seen (blue line). Panels B and C show ΔE^{del}, ΔE^{ins}, and $\Delta E^{del+ins}$. Panel D: the solvent electrostatic potential at the Ru ion positions. Panel E: $\Delta E^{del+ins}$ multiplied by ξ_{ET} (black line, left-hand-side axis) and the difference of the electrostatic potentials between the acceptor and donor ions, $\phi_A - \phi_D$ (red line, right-hand-side axis).

trajectories the ΔE values are zero at $t = 0$, which probably means that our time resolution was not fine enough to see this in the other trajectories. The horizontal dashed line in panel C denotes the average $\langle \Delta E^{del+ins} \rangle = 2.42$ eV from the equilibrium simulation (see also Table 2), which is an indication that our relatively short 2–3 ps trajectories indeed connect the stable reactant and product states, and do not sample only the top region of a free energy barrier.

Another interesting property, already suggested by Marcus, is the solvent electrostatic potential, ϕ_x, $x = $ (D, A) acting on the donor (D) and acceptor (A) ions respectively. These potentials are shown in panel D of Fig. 7. Here, the potentials are approximated by summing the classical Coulomb interaction over all solvent nuclei and associated Wannier centers using the minimum image convention and neglecting the long-range part. The electrostatic potentials are remarkably symmetric with respect to their switching at $t = 0$. Note that all these order

parameters show clearly the barrier recrossing event in path 50 (blue lines) in agreement with the Wannier center position.

Both the $\Delta E^{\mathrm{del+ins}}$ and ϕ_x quantities can be used as reaction coordinates for the electron transfer process. The $\Delta E^{\mathrm{del+ins}}$ parameter does not by itself distinguish between the reactant and product states, as it does not change sign unlike the original ΔE. This can be remedied by keeping track of which of the Ru ions is involved in the electron deletion and insertion processes. Alternatively, the $\Delta E^{\mathrm{del+ins}}$ can be multiplied with ξ_{ET}, which is shown in panel E in Fig. 7 (black line, left-hand-side axis) for the averaged quantities. For the electrostatic potential, we take the difference between ϕ_{A} and ϕ_{D}, which is also shown in panel E (red line, right-hand-side axis). Both these combined order parameters switch smoothly from the reactant state to the product state, crossing zero at $t = 0$.

In Fig. 8, we show the correlation between the three order parameters, by projecting 18 reactive trajectories, taken from the long sequence at an interval of 10, as green points and lines in pairs of the order parameters. The gap energy $\Delta E^{\mathrm{del+ins}}$, multiplied with ξ_{ET}, is shown *versus* the Wannier center position, ξ_{ET}, in the top panel, and *versus* the solvent potential difference, $\phi_{\mathrm{A}} - \phi_{\mathrm{D}}$, in the middle panel. The bottom panel shows $\phi_{\mathrm{A}} - \phi_{\mathrm{D}}$ *versus* ξ_{ET}. Starting with the top panel, we notice that there is a strong correlation between the gap energy and the Wannier center position, and that their relation is not linear. Since ΔE captures the linear response of the solvent polarisation to the amount of charge displaced, the latter being quantified here by ξ_{ET}, this is somewhat surprising. Note however, that ξ_{ET} is obtained from the sampling of adiabatic electron transfer events only (see also Fig. 1, in which the adiabatic profile deviates from the parabolic curves near the barrier). If diabatic electron transfer events could have been included in the statistics of ξ_{ET} at gap energies left and right from the center at $\Delta E = 0$, the curve would have been more straight.

Note also that the fluctuations seen in ΔE in the reactant and product states (*i.e.* at $\xi_{\mathrm{ET}} = -1$ and $\xi_{\mathrm{ET}} = 1$ respectively) disappear at $\xi_{\mathrm{ET}} = 0$. In other words, not only the average gap energy is zero at barrier crossing, but the gap energy for all reactive trajectories is zero at barrier crossing. However, since ΔE (*i.e.* the solvent polarisation) governs the electron position, and not the other way around, this means that a simulation in which the electron position is fixed in the middle, ΔE would exhibit the same fluctuations as it would in the reactant or product state, whereas, *vice versa*, a simulation at fixed $\Delta E = 0$, would show very little fluctuations in the electron position.

Panel B in Fig. 8 shows that there is a good, almost linear, correlation between ΔE and the difference in solvent electrostatic potential. However, the correlation with ξ_{ET} in panel C clearly shows that this potential difference does not uniquely determine the electron position. This could be caused by the approximate nature of the calculation of the electrostatic potential order parameters here, using pairwise sums over nuclei and Wannier center distances, but it could also mean that other interactions play a role. For example, we found that the correlation of ΔE with the solvent electrostatic potential computed using the atomic Mulliken charges would significantly improve when this electrostatic potential was multiplied by a factor depending on the amount of charge transfer from the Ru ion to the aqua ligands in each configuration (data not shown).
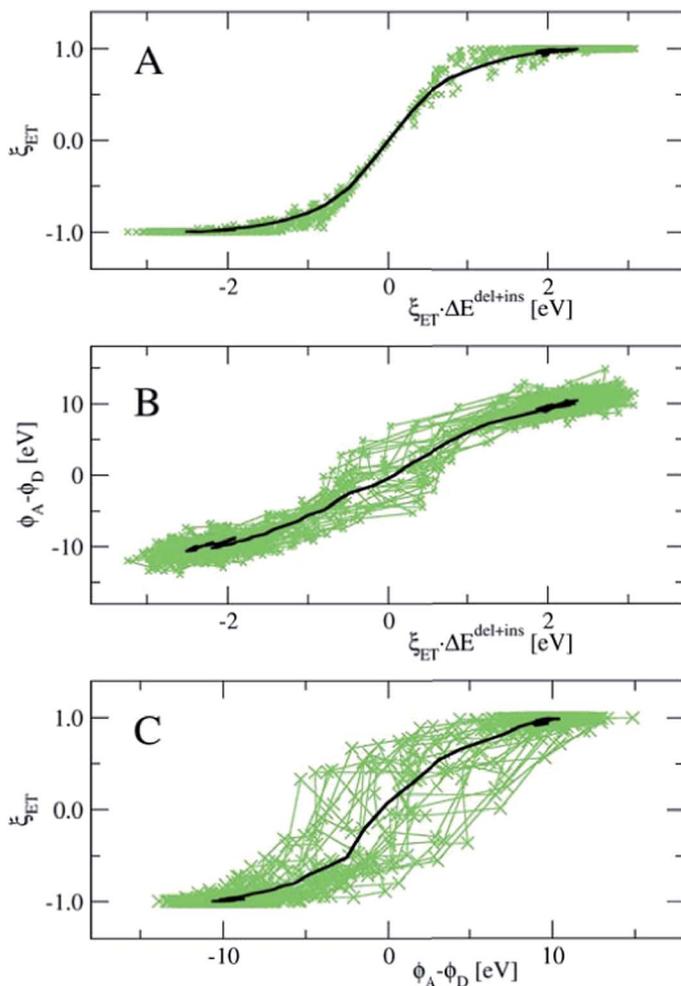
Fig. 8 Correlation between the three reaction coordinations used here to describe the electron transfer reaction. Panel A: the vertical gap energy $\Delta E^{del+ins}$ versus the Wannier center position ξ_{ET}; panel B: $\Delta E^{del+ins}$ versus the difference between the electrostatic potentials at the donor and acceptor ions $\phi_A - \phi_D$; and panel C: $\phi_A - \phi_D$ versus ξ_{ET}. Green crosses and lines denote the points visited along the reactive trajectories; data from 18 paths with an interval of 10 of the longest sequence is used. The black lines show the average over all accepted paths.

3 Conclusions

We have used transition path sampling combined with first principles DFT-MD simulations to investigate the proton-coupled electron transfer reaction taking place between a pair of ruthenium(II/III) ions in aqueous solution. Until now, the main approach to study this prototypical self-exchange reaction at the DFT level of theory was by means of the half-reaction approach. Here, we first applied this approach to construct the diabatic free energy landscape and compute the overall reaction and reorganisation free energies, based on Marcus' linear response

theory of electron transfer. Next, we performed equilibrium DFT-MD simulations of a pair of donor and acceptor ions in solution. As it is not possible for the full reaction to sample the vertical gap energy, ΔE, of transferring the electron from the donor ion to the acceptor ion, the gap energy was probed indirectly as the sum of the energy needed to delete an electron from the donor ion, ΔE^{del}, and the energy required to insert an electron at the acceptor ion, ΔE^{ins}. This allowed us to compute the free energy profiles of the full diabatic electron transfer reaction.

The reactive trajectories generated with DFT-MD/TPS remain always in the electronic ground-state, and thus sample the adiabatic electron transfer landscape. To define the stable reactant and product states, we used as the order parameter, the position of the center of a maximally localised Wannier function associated with the transferring electron. The moment of barrier crossing along each path was set as the reference of the time scale to align the paths and compute averages over the paths. In particular, we have computed the $\Delta E^{del+ins}$ along the electron transfer reaction and also the solvent electrostatic potential at the ruthenium ions, both of which are important ingredients in Marcus' theory of electron transfer.

Correlating the Wannier center position with $\Delta E^{del+ins}$ shows that there is a one-to-one mapping between the order parameters in the neighbourhood of the transition state, where both order parameters pass through zero. This means that the electron position is strictly governed by the value of $\Delta E^{del+ins}$ when it is close to zero. The relation between these two order parameters was surprisingly non-linear however, which we believe to be due to the sampling of only adiabatic electron transfer events. Instead the correlation of the difference between the electrostatic potential at the ruthenium ions shows fluctuations in the electrostatic potential that are not different during electron transfer with respect to that in the stable states. This suggests that the solvent electrostatic potential difference is not a very good reaction coordinate for electron transfer, as it does not determine strictly the amount of electron transfer.

Acknowledgements

References

1 R. A. Marcus, *J. Chem. Phys.*, 1956, **24**, 966.
2 R. A. Marcus, *J. Chem. Phys.*, 1956, **24**, 979–989.
3 R. A. Marcus, *Discuss. Faraday Soc.*, 1960, **29**, 21–31.
4 R. A. Marcus, *J. Chem. Phys.*, 1965, **43**, 679–701.
5 A. Warshel, *J. Phys. Chem.*, 1982, **86**, 2218.
6 J. K. Hwang and A. Warshel, *J. Am. Chem. Soc.*, 1987, **109**, 715.
7 R. A. Kuharski, J. S. Bader, D. Chandler, M. Sprik, M. L. Klein and R. W. Impey, *J. Chem. Phys.*, 1988, **89**, 3248–3257.

8 E. A. Carter and J. T. Hynes, *J. Phys. Chem.*, 1989, **93**, 2184–2187.

9 M. Tachiya, *J. Phys. Chem.*, 1989, **93**, 7050–7052.

10 G. King and A. Warshel, *J. Chem. Phys.*, 1990, **93**, 8682.

11 J. S. Bader, R. A. Kuharski and D. Chandler, *J. Chem. Phys.*, 1990, **93**, 230–236.

12 Q. Wu and T. Van Voorhis, *Phys. Rev. Lett.*, 2005, **72**, 024502.

13 H. Oberhofer and J. Blumberger, *J. Chem. Phys.*, 2009, **131**, 064101.

14 T. Van Voorhis, T. Kowalczyk, B. Kaduk, L.-P. Wang, C.-L. Cheng and Q. Wu, *Annu. Rev. Phys. Chem.*, 2010, **61**, 149–170.

15 I. Tavernelli, R. Vuilleumier and M. Sprik, *Phys. Rev. Lett.*, 2002, **88**, 213002.

16 J. Blumberger, L. Bernasconi, I. Tavernelli, R. Vuilleumier and M. Sprik, *J. Am. Chem. Soc.*, 2004, **126**, 3928–3938.

17 J. Blumberger and M. Sprik, *J. Phys. Chem. B*, 2005, **109**, 6793–6804.

18 J. Blumberger and M. Sprik, *Theor. Chem. Acc.*, 2006, **115**, 113–126.

19 R. Ayala and M. Sprik, *J. Chem. Theory Comput.*, 2006, **2**, 1403–1415.

20 F. Costanzo, M. Sulpizi, R. G. D. Valle and M. Sprik, *J. Chem. Phys.*, 2011, **134**, 244508.

21 P. H.-L. Sit, M. Cococcioni and N. Marzari, *Phys. Rev. Lett.*, 2006, **97**, 028303.

22 J. Blumberger and G. Lamoureux, *Mol. Phys.*, 2008, **106**, 1597–1611.

23 J. VandeVondele, R. Lynden-Bell, E. J. Meijer and M. Sprik, *J. Phys. Chem. B*, 2006, **110**, 3614–3623.

24 J. Cheng, M. Sulpizi and M. Sprik, *J. Chem. Phys.*, 2009, **131**, 154504.

25 M. Kılıç and B. Ensing, *J. Chem. Theory Comput.*, 2013, **9**, 3889–3899.

26 J. Blumberger and M. L. Klein, *J. Am. Chem. Soc.*, 2006, **128**, 13854.

27 J. Blumberger, *Phys. Chem. Chem. Phys.*, 2008, **10**, 5651.

28 B. Ensing, Manuscript submitted.

29 P. G. Bolhuis, D. Chandler, C. Dellago and P. L. Geissler, *Annu. Rev. Phys. Chem.*, 2002, **53**, 291–318.

30 C. Dellago and P. G. Bolhuis, *Mol. Simul.*, 2004, **30**, 795–799.

31 H. Oberhofer and J. Blumberger, *Angew. Chem.*, 2010, **122**, 3713–3716.

32 F. Figueirido, G. S. Del Buono and R. M. Levy, *J. Chem. Phys.*, 1995, **103**, 6133.

33 G. Hummer, L. R. Pratt and A. E. García, *J. Phys. Chem.*, 1996, **100**, 1206–1215.

34 G. Hummer, L. R. Pratt and A. E. García, *J. Chem. Phys.*, 1997, **107**, 9275–9277.

35 P. H. Hünenberger and J. A. McCammon, *J. Chem. Phys.*, 1999, **110**, 1856–1872.

36 N. Marzari, A. A. Mostofi, J. R. Yates, I. Souza and D. Vanderbilt, *Rev. Mod. Phys.*, 2012, **84**, 1419.

37 A. Ambrosetti and P. L. Silvestrelli, Introduction to Maximally Localized Wannier Functions, in *Reviews in Computational Chemistry*, ed. A. L. Parrill and K. B. Lipkowitz, John Wiley & Sons, Inc, Hoboken, NJ, 2016, vol. 29, ch. 6.

38 The CP2K developers group, http://www.cp2k.org.

39 J. VandeVondele, M. Krack, F. Mohamed, M. Parrinello, T. Chassaing and J. Hutter, *Comput. Phys. Commun.*, 2005, **167**, 103–128.

40 G. Lippert, J. Hutter and M. Parrinello, *Mol. Phys.*, 1997, **92**, 477–488.

41 S. Goedecker, M. Teter and J. Hutter, *Phys. Rev. B: Condens. Matter Mater. Phys.*, 1996, **54**, 1703.

42 A. D. Becke, *Phys. Rev. A*, 1988, **38**, 3098–3100.

43 C. T. Lee, W. T. Yang and R. G. Parr, *Phys. Rev. B: Condens. Matter Mater. Phys.*, 1988, **37**, 785–789.

44 S. Grimme, *J. Comput. Chem.*, 2004, **25**, 1463–1473.

45 S. Grimme, *J. Comput. Chem.*, 2006, **27**, 1787–1799.

46 J. Schmidt, J. VandeVondele, I.-F. W. Kuo, D. Sebastiani, J. I. Siepmann, J. Hutter and C. J. Mundy, *J. Phys. Chem. B*, 2009, **113**, 11959–11964.

47 M. J. Gillan, D. Alfè and A. Michaelides, *J. Chem. Phys.*, 2016, **144**, 130901.

48 G. Bussi, D. Donadio and M. Parrinello, *J. Chem. Phys.*, 2007, **126**, 014101.

49 F. P. Rotzinger, *J. Chem. Soc., Dalton Trans.*, 2002, 719–728.

50 P. Bernhard, L. Helm, A. Ludi and A. E. Merbach, *J. Am. Chem. Soc.*, 1985, **107**, 312–317.